Journal of Turbulence
Volume 7, No. 41, 2006

Scale dependence of the coarse-grained velocity derivative tensor: Influence of large-scale shear on small-scale turbulence

AURORE NASO†‡§, MICHAEL CHERTKOV§ and ALAIN PUMIR*†

†Institut Non Linéaire de Nice (U.M.R. C.N.R.S 6618), Université de Nice Sophia Antipolis, 1361 Route des Lucioles, F-06560 Valbonne, France
‡Department of Applied Physics, University of Twente, P.O. Box 217, 7500 AE Enschede, The Netherlands
§Center for Nonlinear Studies and Theoretical Division, Los Alamos National Laboratory, NM 87545, USA

We discuss the effect of large-scale anisotropy of the shear type on the small-scale structure of turbulence. Our analysis is based on numerical solutions of the Lagrangian tetrad model of Chertkov M., Pumir A. and Shraiman B.I. (1999, *Physics of Fluids*, **11**, 2394) adapted to the model case with large-scale anisotropy. The model, formulated in terms of a set of stochastic differential equations for the coarse-grained velocity gradient and tensor of inertia of a typical shape, naturally connects Lagrangian and Eulerian parameterizations of turbulence. We use diagnostics of Chertkov *et al.* (1999) which allows us to analyse and interpret different correlation functions at the resolved scale in terms of the flow geometry. Our main conclusion, concerning the issue of anisotropy, is that even though overall the local isotropy is restored with the scale decrease, the particular pace of the isotropy restoration depends very much on the object analysed. We found that the vorticity-dominated objects, such as enstrophy, tend to restore the isotropy much faster than their strain-dominated counterparts, e.g. energy flux and strain variance.

Keywords: Shear turbulence; flow topology; phenomenological models

1. Introduction

The dynamics of velocity fluctuations in turbulent flows is characterized by remarkable power-laws, describing the scale dependence of the correlation functions. The most famous example is the $k^{-5/3}$ energy spectrum [1] which has been derived originally in a situation where the flow properties are statistically homogeneous and isotropic [2]. This highly idealized case turns out to provide a very deep insight into the structure of turbulent flows. Nevertheless, deviations from the idealized case are expected when the flow is anisotropic and/or inhomogeneous, as in essentially any flow of natural or engineering relevance.

In fact, most flows are generated by a large-scale forcing, which generally breaks the isotropy and homogeneity symmetries at the largest scales. Simple theoretical reasoning, as well as decades of careful experimental work has suggested that symmetry is restored at the smallest scales of the motion [3, 4]. One of the simplest flow configurations to study this effect is the

*Corresponding author. E-mail: Alain.Pumir@inln.cnrs.fr

Journal of Turbulence
ISSN: 1468-5248 (online only) © 2006 Taylor & Francis
http://www.tandf.co.uk/journals
DOI: 10.1080/14685240600754563

so-called homogeneous turbulent shear flow, where the velocity field can be decomposed as $\vec{U} = (sy, 0, 0) + \vec{u}$, where s is the mean shear, and the fluctuating velocity $\vec{u}$ has a zero mean value: $\langle \vec{u} \rangle = 0$. In this configuration, odd moments of $\partial_y u_x$, which would be zero if the flow were strictly isotropic, remain large even at very small scales, and at very large Reynolds numbers [5], a phenomenon anticipated in [6, 7]. However, the influence of the anisotropy on other moments, which are non-zero in the case of a strictly isotropic flow, decays as the spatial scale decays, and as the Reynolds number increases [4].

In this work, we reconsider the problem of the interaction between a large-scale shear and small-scale turbulent fluctuations. The idealized flow studied is homogeneous, but the mean shear induces a large-scale anisotropy. The aim here is to investigate the structure of the velocity gradient tensor as a function of scale and of the externally applied shear s. Our description is based on the invariants of the coarse-grained velocity gradient tensor. More precisely, if $\hat{m}$ is the velocity gradient tensor: $m_{ab} = \partial_a v_b$, one defines the velocity gradient tensor coarse grained over a region Γ of size r, $M_{ab} = (1/V_r) \int_\Gamma m_{ab} \mathrm{d}^3 x$, where $V_r \sim r^3$. This tensor is traceless, and its topological properties can be characterized by the two invariants [8], Q and R:

$$Q = -\frac{1}{2}\mathrm{Tr}(\hat{M}^2), \quad R = -\frac{1}{3}\mathrm{Tr}(\hat{M}^3). \tag{1}$$

The smallest number of points one needs to extract the coarse-grained velocity gradient from direct numerical simulation (DNS) or experimental data is 4; thus the minimal model introduced in [9] was formulated in terms of tetrad—the 4-points tetrahedron. Effectively, studying the structure of the $\hat{M}$-tensor is equivalent to asking questions about the structure of the correlation function of the velocity field at four points (or more), separated by a characteristic scale r. Experiments in this spirit have been carried out in the case of a passive scalar in the presence of a mean gradient [10], and can be carried out with multi-wire probes [11], or with PIV devices [12].

Describing the velocity fluctuations from first principles remains an essentially impossible task, despite the recent progress made in the related problem of passive advection by a turbulent velocity field [13]. Even in this simpler problem, progress came from the analysis of simpler models, such as the Kraichnan model of turbulence [14]. The present work is based on the modelling approach developed in [9], which reduces the turbulence problem to a set of stochastic differential equations, and to a computationally efficient semi-classical analysis of the resulting Fokker–Planck equation [15]. Fokker–Planck describes evolution of the probability distribution function (PDF) of the coarse-grained $\hat{M}$ over scales. The semi-classical trajectory has a clear meaning of the most probable Lagrangian path bringing correlations from the large (integral) scale to the observation scale r in the inertial range. The large-scale anisotropy is introduced by assuming an anisotropic form for the PDF of $\hat{M}$ at the integral scale. Specifically the coarse-grained velocity gradient at the integral scale is assumed to have a Gaussian distribution, around the mean value $M_{ab} = \delta_{a2}\delta_{b1}s$.

The model involves three dimensionless parameters characterizing the reduction of the nonlinearity induced by the pressure term, the re-isotropization effect of the small-scale velocity field and the influence of the small scales on the coarse-grained velocity derivative tensor, respectively. In this work, we use the values of the parameters determined in [15].

The main result of this work is that the general relaxation towards the isotropic situation as scale decreases proceeds faster for vorticity-dominated correlation functions than for strain-dominated ones.

The model is briefly introduced in section 2. The results expressed in terms of conditional densities projected to the plane of the invariants, (Q, R), are discussed in section 3. Finally, section 4 presents our concluding remarks.

2. Formulation of the model and method of resolution

In this section, we briefly recall the derivation of the tetrad model [9]. We use it to introduce notation, emphasize key parameters and discuss methods of analysis. The novel aspect compared to the previous work [9, 15] comes from the anisotropy condition for the PDF imposed at the integral scale.

2.1. *Formulation of the model*

The model is formulated in terms of the traceless matrix $\hat{M}$, defining the coarse-grained velocity derivative, and the symmetric matrix $\hat{g}$ introduced for the tetrad tensor of inertia. The starting point of our approach consists in describing the Lagrangian evolution of $\hat{M}$ and $\hat{g}$ in terms of the following set of equations:

$$\frac{\mathrm{d}\hat{M}}{\mathrm{d}t} + (1-\alpha)(\hat{M}^2 - \hat{\Pi}\,\mathrm{Tr}\hat{M}^2) = \hat{\eta}, \tag{2}$$

$$\hat{\Pi} \equiv \hat{g}^{-1}/\mathrm{Tr}\,(\hat{g}^{-1}), \tag{3}$$

$$\frac{\mathrm{d}\hat{g}}{\mathrm{d}t} - \hat{g}\hat{M} - \hat{M}^t\hat{g} - \beta\sqrt{\mathrm{Tr}(\hat{M}\hat{M}^t)}\left(\hat{g} - \frac{\mathrm{Tr}(\hat{g})}{3}\hat{1}\right) = 0, \tag{4}$$

$$\langle \eta_{ab}\,(\rho;t)\,\eta_{cd}\,(0;0)\rangle = \gamma\left(\delta_{ac}\delta_{bd} - \frac{1}{3}\delta_{ab}\delta_{cd}\right)\frac{\varepsilon}{\rho^2}\delta\,(t)\,, \tag{5}$$

where $\rho^2 = \mathrm{Tr}(\hat{g})$. Aside from the dimensional quantity ε, the energy dissipation, the model involves three dimensionless parameters, α, β and γ.

These phenomenological equations can be justified by considering a tetrahedron of Lagrangian particles, whose positions are $\vec{r}_i$ $(i = 1, \ldots, 4)$. The motion of the centre-of-mass of the set of points, $\vec{\rho}_0 = \sum_i \vec{r}_i$ does not play any role, because of the assumed homogeneity of the flow. As a consequence, the geometry of the tetrad is described by a set of three reduced coordinates, $\vec{\rho}_i$. The above model is formulated in terms of the moment of inertia tensor $g_{ab} = \sum_i \rho_i^a \rho_i^b$, defined with the help of the reduced coordinate tensor ρ_i^a.

In deriving the equation for the coarse-grained velocity derivative tensor, $\hat{M}$, a number of assumptions have to be made about the pressure Hessian tensor. Numerical results [9, 16] suggest that the pressure Hessian tensor reduces the nonlinearity in the equation—the effect which is captured by the dimensionless parameter α in equation (2). The incompressibility condition, $\mathrm{Tr}(\hat{M}) = 0$, is obtained by subtracting directly $\mathrm{Tr}(\hat{M}^2)\hat{\Pi}$, where $\hat{\Pi}$ is a matrix such that $\mathrm{Tr}(\hat{\Pi}) = 1$. The particular choice of $\hat{\Pi}$, equation (3), can be justified in the case of a homogeneous isotropic flow from an energy balance, using the fact that pressure does not do any work [9], and by the fact that this particular choice prevents the solution from blowing-up in a finite time in the deterministic case ($\hat{\eta} = 0$). Another justification for the specific form of $\hat{M}$ in the general case comes from the requirement for the $\hat{g}$ tensor to preserve the Hamiltonian structure for an ideal tetrad dynamics [17]. The stochastic term models the effect of the rapidly fluctuating small-scale effects on the pressure. It is assumed to be Gaussian, white in time, with a scaling form consistent with the Kolmogorov's 4/5-law. Its intensity is simply measured by the dimensionless factor γ.

Equation (4) for the tensor of inertia describes advection of the points by the coarse-grained velocity tensor, $\hat{M}$, and it also accounts for the diffusive, isotropization effect of velocity fluctuations from the scales smaller than the one of coarse graining. The former term leads to the direct coupling between $\hat{M}$ and $\hat{g}$ in equation (4). The latter similar contribution, to

the noise term $\hat{\eta}$ in equation (2), can be modelled by short-correlated in time noise term. However, a more refined analysis of this fluctuating term [18, 19] shows that its main effect is to counteract the tendency of the stretching term, $\hat{g}\hat{M}$, to generate very anisotropic shapes. For this reason and also seeking for simpler modelling, the noise term is replaced by the β-term in equation (4), which effectively counterbalances the stretching term and tends to restore the isotropy [15].

The model thus reduces to a set of stochastic differential equations, which, aside from the dimensional parameter ε, the rate of energy dissipation, involves three dimensionless parameters: α, which controls the reduction of nonlinearity, β, which controls dynamical isotropization of the tetrad shape and γ, characterizing the strength of the noise term in the $\hat{M}$-equation.

As stated above, the large-scale anisotropy is imposed by our choice of PDF at the integral scale. Numerous experimental and numerical studies indicate that the velocity field is Gaussian at scales larger than the integral scale, L. For homogeneous, isotropic turbulent flow considered in [9, 15], the condition imposed at L was $P(\hat{M}, \mathrm{Tr}(\hat{g}) = 3L^2) \sim \exp[-\mathrm{Tr}(\hat{M}\hat{M}^t)/(\varepsilon L^{-2})^{2/3}]$. In the presence of a large-scale gradient, we assume for the coarse-grained velocity derivative tensor to still show a Gaussian PDF, with non-zero mean described by the mean shear, $\hat{\Sigma}$:

$$P(\hat{M},\ \mathrm{Tr}(\hat{g}) = L^2) \sim \exp\left[-\frac{\mathrm{Tr}[(\hat{M}-\hat{\Sigma})(\hat{M}-\hat{\Sigma})^t]}{\varepsilon^{2/3}L^{-4/3}}\right] \tag{6}$$

$$\hat{\Sigma} = \begin{pmatrix} 0 & 0 & 0 \\ s & 0 & 0 \\ 0 & 0 & 0 \end{pmatrix}. \tag{7}$$

2.2. *Method of resolution*

The probability distribution function (PDF) describing the distribution of the matrices $\hat{M}$ and $\hat{g}$, $P(\hat{M}, \hat{g})$, as a function of time, obeys a Fokker–Planck (FP) equation. In the steady-state case, considered here, the solution of the FP equation can be formally expressed as a path integral:

$$\begin{aligned} P(\hat{M}, \hat{g}) = &\int \mathrm{d}\hat{M}' \int \mathrm{d}T \int_{\hat{M}''(-T)=\hat{M}'}^{\hat{M}''(0)=\hat{M}} [\mathcal{D}\hat{M}''] \int_{\hat{g}''(-T)=\hat{g}'}^{\hat{g}''(0)=\hat{g}} [\mathcal{D}\hat{g}''] \\ &\exp\left[-\frac{\mathrm{Tr}[(\hat{M}'-\hat{\Sigma})(\hat{M}'-\hat{\Sigma})^t]}{\varepsilon^{2/3}L^{-4/3}} - \mathcal{S}(\hat{M}''; \hat{g}'')\right] \\ &\times \delta\left(\frac{\mathrm{d}\hat{g}''}{\mathrm{d}t} - \hat{g}''\hat{M}'' - [\hat{M}'']^t\hat{g}'' - \beta\sqrt{\mathrm{Tr}(\hat{M}''[\hat{M}'']^t)}\left(\hat{g}'' - \frac{\mathrm{Tr}(\hat{g}'')}{3}\hat{1}\right)\right), \end{aligned} \tag{8}$$

where $\mathcal{S}$ is the 'classical' action:

$$\mathcal{S} = \int_0^T \mathrm{d}t\ \frac{\mathrm{Tr}\left[D_{\hat{M}} D_{\hat{M}}{}^t\right]}{2\gamma\varepsilon/\rho^2}, \tag{9}$$

where

$$D_{\hat{M}} = \frac{\mathrm{d}\hat{M}''}{\mathrm{d}t} + (1-\alpha)\,([\hat{M}'']^2 - \hat{\Pi}''\,\mathrm{Tr}[\hat{M}'']^2). \tag{10}$$

In accordance with explanations of the previous section matrices, $\hat{M}''$ and $\hat{g}''$ are considered to be traceless and symmetric respectively. A standard numerical way to evaluate the path integral (8) is through a Monte Carlo simulation. However, the direct Monte Carlo is extremely

costly, especially taking into account that we want to explore $P(\hat{M}, \hat{g})$ at different scales, parameterized by $\mathrm{Tr}[\hat{g}]$, and different values of $\hat{M}$.

Following the approach developed in [15], equation (8) is instead approximated in a semi-classical way. In this approach, which is essentially equivalent to a saddle-point method, one estimates an integral by the largest possible value of its integrand. The action term, equations (9), (10), is of the form $\int_0^T \mathcal{L}\mathrm{d}t$, so the extremum of the action can be estimated by solving the variational Euler–Lagrange equations, $\delta\mathcal{L} = 0$, considering the matrices and their derivatives as independent. The extremum is found by the algorithm 'amebsa' [15, 20], a simplex method combined with a simulated annealing algorithm. Minimization of the action $\mathcal{S}$ in equations (9), (10) goes over the set of initial conditions for $\mathrm{d}\hat{M}/\mathrm{d}t$ and $\mathrm{d}\hat{g}/\mathrm{d}t$ and also over some number of initial degrees of freedom in $\hat{M}$ inessential for our $Q - R$ plane diagnostics, see [15] for details. For any individual realization we run the Euler–Lagrange equations and respective equations for $\hat{g}''$ backwards in time from $t = 0$ till $-T$, defined as $r(-T) = L$. The only difference with the algorithm developed in [15] comes from the implementation of the large-scale condition (6). The convergence of the algorithm is satisfactory.

2.3. *Choice of the model parameters*

As already explained, the model equations involve one-dimensional parameter (ε, the energy dissipation) and the three dimensionless parameters α, β and γ, introduced before. The large-scale condition (equation (6)) introduces an extra-dimensional parameter: L, the integral scale. The values of ε and L can be taken as 1, by a proper rescaling of temporal and spatial units. The dimensionless parameters have to be fixed based on other considerations.

It was shown in [15] that the resulting data (for PDF and correlation functions) are sensitive to the choice of the value of α, which measures the pressure-induced reduction of nonlinearity. It was found that the results of the model are physically sensible only when the value of α is in a narrow interval around $\alpha \sim 0.5$. The effect of two other parameters, β and γ, on the model's predictions was found to be weaker.

Guided by the numerical findings of [15], we have chosen here $\alpha = 0.6$, $\beta = 0.4$ and $\gamma = 0.25$.

The value of the applied (large-scale) shear, s, can be made dimensionless by the following rescaling:

$$S^* = s(L^2/\varepsilon)^{1/3}. \tag{11}$$

In the following, the units of time and scale are chosen in such a way that L and ε are both equal to 1. The value of s (equal to S^*) thus measures directly the effect of the external shear on the turbulence intensity. In turbulent shear flows' experiments or numerical simulations, the value of S^* has been found to vary in a broad interval of values $3 \lesssim S^* \lesssim 10$ [21]. We consider here the purely isotropic case ($S^* = 0$), a weakly anisotropic case ($S^* = 1$) and a more strongly anisotropic case ($S^* = 6$).

3. Numerical results

We present in this section the predictions of the model.

Our analysis rests very much on the study of PDF in the (R, Q) plane. This representation allows a discussion of the topology of the flow [8]. The discriminant $D = 27R^2 + 4Q^3$ allows us to characterize the eigenvalues of the coarse-grained velocity derivative tensor. The flow is hyperbolic (elliptic) in the sense that the matrix $\hat{M}$ has three real eigenvalues (one real,

and two complex conjugate eigenvalues) when $D < 0$ ($D > 0$). The probability distribution function is very skewed along the line with positive values of R, zero discriminant (PRZD line), a phenomenon qualitatively consistent with the model equations, equations (2)–(5).

3.1. *Probability distribution functions in the (R, Q) plane*

The joint PDFs of (R, Q) are shown in figure 1 for different values of r ($r/L = 1/2$, figure 1(a), $r/L = 1/4$, figure 1(b), $r/L = 1/8$, figure 1(c) and $r/L = 1/16$, figure 1(d)). The R and Q invariants are normalized in terms of the scale, r, and of the energy dissipation rate, ε. Thus, $Q_r = Q \times (r^2/\varepsilon)^{2/3}$ and $R_r = R \times (r^2/\varepsilon)$, for three different values of S^*: $S^* = 0$ (red), $S^* = 1$ (green) and $S^* = 6$ (blue). Isoprobability lines are logarithmically spaced, and separated by factors of 10.

In discussing these figures it is important to keep in mind that the computed coarse-grained velocity derivative tensor includes the mean shear, $\hat{\Sigma}$. As a result, the overall size of the velocity

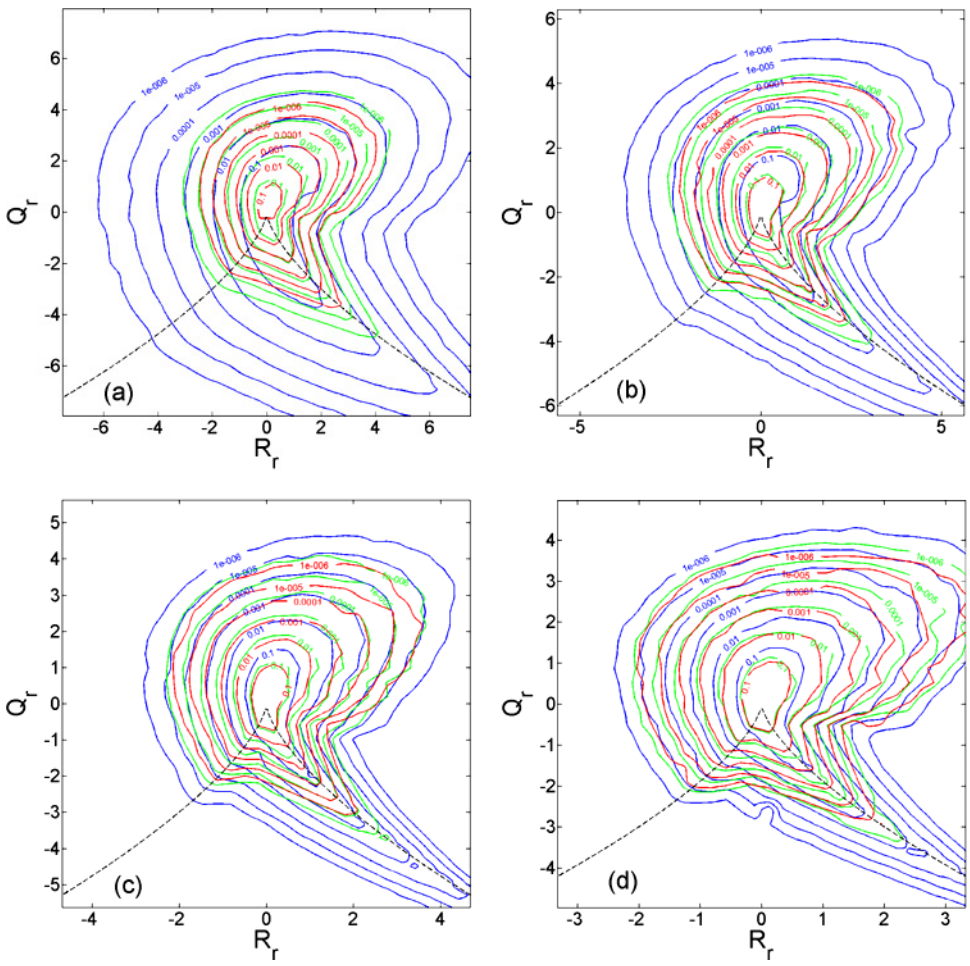

Figure 1. PDF of the normalized Q_r,R_r invariants: $Q_r = Q \times (r^2/\varepsilon)^{2/3}$, $R_r = R \times (r^2/\varepsilon)$, for $\alpha = 0.6$, $\beta = 0.4$, $\gamma = 0.25$ and $S^* = 0$ (red), 1 (green), 6 (blue): (a) $r = L/2$, (b) $r = L/4$, (c) $r = L/8$, (d) $r = L/16$. The isoprobability contours are logarithmically spaced, and separated by factors of 10.

fluctuations is markedly larger, in particular at large values of S^*, and at large values of r/L. As the value of r/L decreases, the relative importance of the imposed mean shear diminishes, so the isoprobability contours corresponding to the different values of S^* generally tend to get closer to one another. Even so, even at fairly small values of r/L ($r/L = 1/16$, see figure 1(d)), the probability distribution functions remain very significantly different along the PRZD line. This result suggests that the rate of relaxation to isotropy predicted by the model actually depends on the kind of structure one is considering. Vortex-dominated regions, located in the upper part of the (R, Q)-plane ($Q > 0$), seem to relax to isotropy much faster than strain-dominated regions, located around the PRZD line.

3.2. *Scaling laws for strain and vorticity*

The difference in relaxation between vortex-dominated regions and strain-dominated regions can be quantified by measuring the scale dependences of the strain, $\mathrm{Tr}(\hat{S}^2)$, and of the vorticity, ω^2, as a function of scale, r, for different values of S^*. As usual, the strain (vorticity) is defined as the symmetric (antisymmetric) part of the (coarse-grained) velocity derivative tensor: $\hat{S} = (\hat{M} + \hat{M}^t)/2$, $\omega_i = \varepsilon_{ijk} M_{jk}$.

The quantities $\langle \mathrm{Tr}(\hat{S}^2) \rangle$ and $\langle \omega^2 \rangle$ are shown in figure 2. Consistent with the results of [15], these invariants follow very well Kolmogorov predictions ($\langle \mathrm{Tr}(\hat{S}^2) \rangle, \langle \omega^2 \rangle \sim r^{-4/3}$) in the absence of external shear ($S^* = 0$). As anticipated from figure 1, in the presence of a mean shear, the values of the vorticity relax quickly at small scales towards the isotropic values ($S^* = 0$), see figure 2(a). This tendency is also obvious in the compensated plot of $r^{4/3}\omega^2$ (figure 2(b)). The situation is significantly different for the value of $\langle \mathrm{Tr}(\hat{S}^2) \rangle$, which seems to relax much more slowly, towards the values obtained at $S^* = 0$, figure 2(c). The very slow

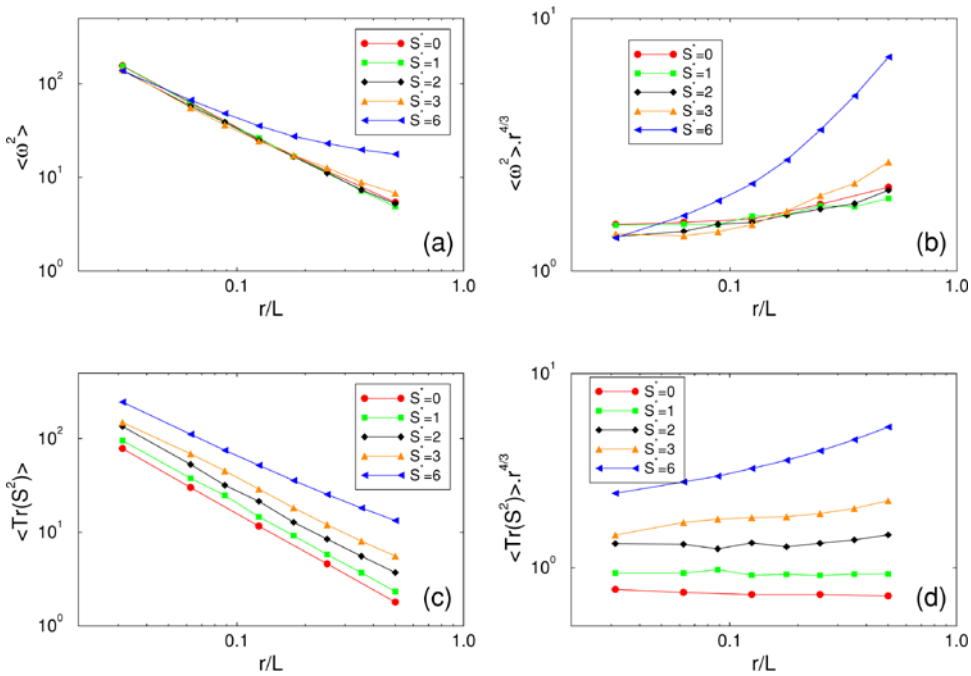

Figure 2. Scaling laws of (a) and (b) $\langle \omega^2 \rangle$, (c) and (d) $\langle Tr(\hat{S}^2) \rangle$ for $\alpha = 0.4$, $\beta = 0.4$, $\gamma = 0.25$, and $S^* = 0, 1, 2, 3, 6$. In (b) and (d) the scaling laws are compensated by the K41 prediction in the isotropic case, $r^{-4/3}$.

relaxation towards the Kolmogorov scaling can be seen in figure 2(d) plotting $\langle \mathrm{Tr}(\hat{S}^2)\rangle \times r^{4/3}$ as a function of r.

The results of the two previous subsections therefore demonstrate that the model predicts a very different relaxation towards isotropy, depending on which structure is actually investigated. Vorticity-dominated structures here seem to relax better towards isotropy when the scale r/L decreases, than strain-dominated regions.

3.3. *Densities in the (R, Q) plane*

The distribution of quantities of dynamic relevance, such as enstrophy (ω^2), strain intensity ($\mathrm{Tr}(\hat{S}^2)$) as well as energy production ($-r^2\mathrm{Tr}(\hat{M}^2\hat{M}^t)$, see [9]) is of general interest to understand the dynamics of turbulent flows [11]. These quantities have been studied both by DNS at moderate Reynolds number [9], and using the model [15]. We study here the influence of a mean shear S^* and of the scale r on these distributions.

Figure 3 shows the density of enstrophy, figure 4 the density of strain and figure 5 the density of the energy transfer, for the three values of $S^* = 0$, 1 and 6, and at scales $r/L = 1/4$ (a) and $r/L = 1/16$ (b).

The general effect of the imposed mean shear, S^*, is to shift the location where the densities of the dynamical quantities shown in figures 3–5 are maximal away from the origin in the (Q, R) plane, towards the PRZD line. The effect for the enstrophy, figure 3, is visible only at moderate scales ($r/L = 1/4$), less so at smaller scales ($r/L = 1/16$). On the other hand, the effect remains very strong for the strain (figure 4) and for the energy transfer (figure 5), even at our smallest values of the scale. The fact that strain-dominated quantities relax less quickly towards isotropy than vorticity-dominated quantities, observed in the previous subsections, certainly explains the tendency observed here. The energy transfer is a strain-dominated quantity, so it is natural to expect that this quantity relaxes slowly to isotropy at small scales.

Figure 6 shows the mean energy transfer dependence as a function of r. As it was the case for the strain, see figures 2(c)–(d), the relaxation towards the isotropic values at small scales is very low.

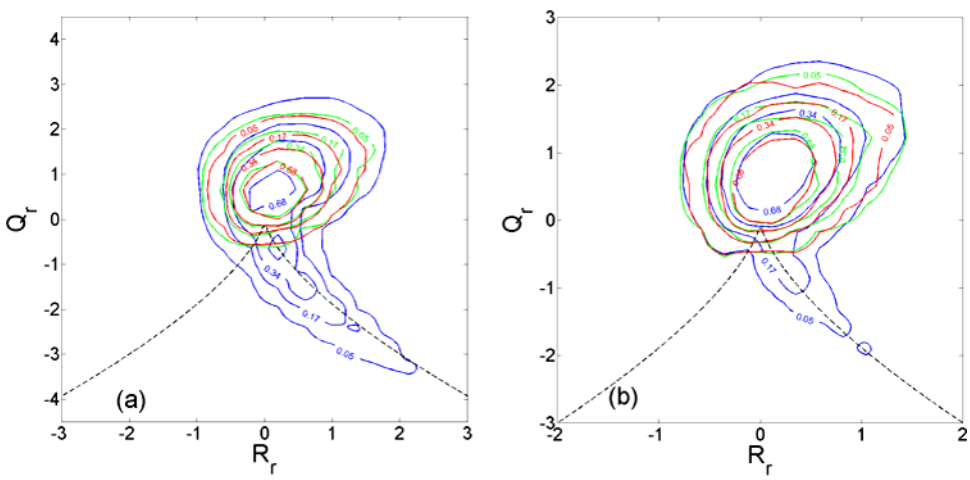

Figure 3. Enstrophy densities in the (R_r, Q_r) plane, normalized by $\langle \mathrm{Tr}(\hat{S}^2)\rangle$. The densities are calculated for $\alpha = 0.6$, $\beta = 0.4$, $\gamma = 0.25$, and $S^* = 0$ (red), 1 (green), 6 (blue): (a) $r/L = 1/4$ and (b) $r/L = 1/16$. The values of the isoprobability lines are 0.68, 0.34, 0.17 and 0.05.

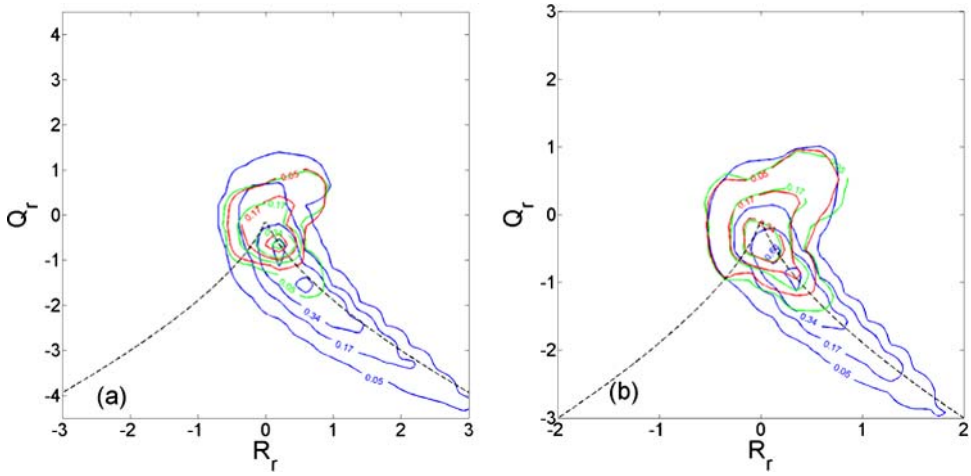

Figure 4. $\mathrm{Tr}(\hat{S}^2)$ densities in the (R_r, Q_r) plane, normalized by $\langle \mathrm{Tr}(\hat{S}^2)\rangle$. The conventions are the same as in figure 3. The values of the isoprobability lines are 0.68, 0.34, 0.17 and 0.05.

3.4. *Discussion*

The notion that correlation functions probing different geometric structures should behave differently had been already noted, even in an isotropic context [22, 23]. It is also expected, from a theoretical point of view, that the rates of decay of correlation functions towards isotropy depend on the precise object studied.

The numerical results, obtained here with the tetrad model of turbulence, are consistent with the accepted view [4] that the effect of the anisotropy imposed at large scale tends to decrease when the scale r decreases. The diagnostics used here suggest new insight into the physical aspects of relaxation towards small scales. The results of the model point towards an interesting difference between strain- and vorticity-dominated structures. The latter tend to

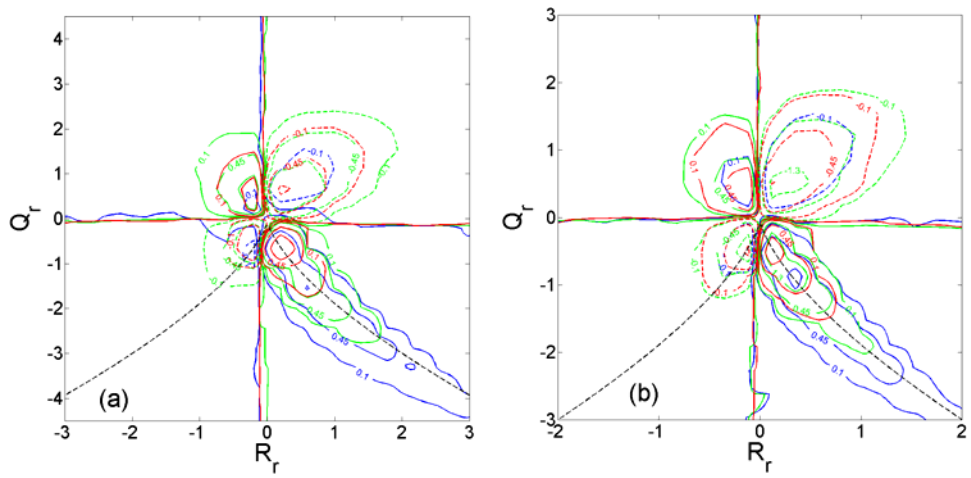

Figure 5. Energy transfer $-r^2\mathrm{Tr}(\hat{M}^2\hat{M}^t)$ densities in the (R_r, Q_r) plane, normalized by $|\langle -r^2\mathrm{Tr}(\hat{M}^2\hat{M}^t)\rangle|$. The conventions are the same as in figure 3. The values of the isoprobability lines are 1.3, 0.45, 0.1, 0, −0.1, −0.45 and −1.3. The dashed lines indicate negative values.

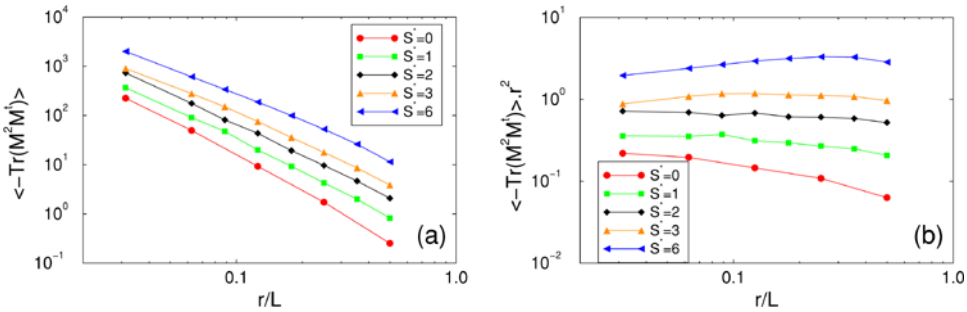

Figure 6. Scaling laws of (a) the energy transfer divided by r^2 and (b) the energy transfer $\langle -r^2 \mathrm{Tr}(\hat{M}^2 \hat{M}^t) \rangle$ for $\alpha = 0.4$, $\beta = 0.4$, $\gamma = 0.25$, and $S^* = 0, 1, 2, 3, 6$.

'forget' faster about the large-scale anisotropy than the former, as the scale r decreases. This qualitative result is independent of the order of the correlation function investigated (we have mostly considered here moments of orders 2 and 3 only).

The faster relaxation of vorticity-dominated structures towards isotropy is consistent with the observation that vortical structures in turbulent flows are generally much more intense than strain structures. As a result, they are intrinsically less sensitive to a moderate, large-scale effect, such as an imposed shear.

4. Conclusion

We have investigated here the effect of a simple large-scale flow on the structure of the coarse-grained velocity derivative tensor, with the help of the tetrad model of turbulence [9]. Solutions were computed here with the semi-classical approach, used so far only in a purely isotropic situation [15]. It was shown that the model reproduces qualitatively, and even semi-quantitatively, the well-documented trends obtained in homogeneous isotropic turbulence.

As it has been documented in other contexts, our numerical results are consistent with the fact that the corrections to isotropy tend to decrease as the scale decreases. The main result of this work is that anisotropy decreases significantly faster for vorticity-dominated structures than for strain-dominated structures. The conclusions obtained here with the tetrad model ultimately call for tests, from experiments and/or direct numerical simulations. It would be instructive to investigate the structure of the probability distribution function of the invariants (R, Q) as a function of scale, and see whether the effects presented in this paper can indeed be observed in a real flow. In any case, experimental results based on a well-controlled flow, or on a DNS would provide more stringent tests on the tetrad model.

This work is the first attempt to study the tetrad model in a context more relevant to engineering flows. From a theoretical point of view, the large-scale shear only modifies the conditions at large scale, equation (6), compared to the already studied homogeneous isotropic case. Other relatively simple geometric configurations, such as a well-controlled contraction/extension, could be studied in a similar manner. Recent experimental results for this problem [24] suggest a very rich phenomenology, which is well worth studying, e.g. through the tetrad modelling. Another prominent direction for the modelling research lies in analysing inhomogeneous and possibly non-stationary turbulent flows. To describe dynamics and statistics in the complex flows one needs to find a way of explaining simultaneously ballistic (coherent) and turbulent (diffusive) transport. Properly modified and generalized Lagrangian tetrad model can be capable of providing a satisfactory description for the complex situations. A particularly interesting area of research where this approach may apply and essentially improve the existing phenomenology [25] is Rayleigh–Taylor turbulence.

References

[1] Kolmogorov, A.N., 1941, The local structure of turbulence in incompressible viscous fluid for very large Reynolds numbers. *Comptes Rendus de l'Academie des Sciences, USSR,* **30**, 301.

[2] Frisch, U., 1995, *Turbulence: The Legacy of AN Kolmogorov* (Cambridge: Cambridge University Press).

[3] Sreenivasan, K., 1991, On local isotropy of passive scalars in turbulent shear flows. *Proceedings of the Royal Society of London, Series A,* **434**, 165.

[4] Biferale, L. and Procaccia, I., 2005, Anisotropy in turbulent flows and in turbulent transport. *Physics Reports*, **414**, 43.

[5] Shen, X. and Warhaft, Z., 2000, The anisotropy of the small scale structure in high Reynolds numbers turbulent shear flows. *Physics of Fluids*, **12**, 2976.

[6] Pumir, A. and Shraiman, B.I., 1995, Persistent small scale anisotropy in homogeneous shear flows. *Physical Review of Letters*, **75**, 3114.

[7] Pumir, A., 1996, Turbulence in homogeneous shear flows. *Physics of Fluids*, **8**, 3112.

[8] Cantwell, B.J., 1992, Exact solution of a restricted Euler equation for the velocity gradient tensor. *Physics of Fluids A*, **4**, 782.

[9] Chertkov, M., Pumir, A. and Shraiman, B.I., 1999, Lagrangian tetrad dynamics and the phenomenology of turbulence. *Physics of Fluids*, **11**, 2394.

[10] Mydlarski, L., Pumir, A., Shraiman, B.I., Siggia, E.D. and Warhaft, Z., 1998, Structures and multipoint correlators for turbulent advection: predictions and experiments. *Physical Review of Letters*, **81**, 4373.

[11] Kholmyansky, M., Tsinober, A. and Yorish, S., 2001, Velocity derivatives in the atmospheric surface layer. *Physics of Fluids*, **13**, 311.

[12] Van der Bos, F., Tao, B., Meneveau, C. and Katz, J., 2002, Effects of small-scale turbulent motions on the filtered velocity gradient tensor as deduced from holographic particle image velocimetry measurements. *Physics of Fluids*, **14**, 2456.

[13] Falkovich, G., Gawedzki, K. and Vergassola, M., 2001, Particles and fields in fluid turbulence. *Reviews of Modern Physics*, **73**, 913.

[14] Kraichnan, R.H., 1968, Small-scale structure of a scalar convected by turbulence. *Physics of Fluids*, **11**, 945.

[15] Naso, A. and Pumir, A., 2005, Scale dependence of the coarse-grained velocity derivative tensor structure in turbulence. *Physical Review E*, **72**, 056318.

[16] Borue, V. and Orszag, S.A., 1998, Local energy flux and subgrid scale statistics in three-dimensional turbulence. *Journal of Fluid Mechanics*, **366**, 1.

[17] Chertkov, M. and Pumir, A., 2006, Large Eddy simulations based on Lagrangian tetrad modeling, in preparation.

[18] Pumir, A., Shraiman, B.I. and Chertkov, M., 2000, Geometry of Lagrangian dispersion in turbulence. *Physical Review of Letters*, **85**, 5324.

[19] Biferale, L., Boffetta, G., Celani, A., Devenish, B.J., Lanotte, A. and Toschi, F., 2005, Multi particle dispersion in fully developed turbulence. *Physics of Fluids*, **17**, 111701.

[20] Press, W.H., Teukolsky, S.A., Vetterling, W.T. and Flannery, B.P., 1992, *Numerical Recipes in C* (Cambridge: Cambridge University Press), p. 451.

[21] Schumacher, J., Sreenivasan, K.R. and Yeung, P.K., 2003, Derivative moments in turbulent shear flows. *Physics of Fluids*, **15**, 84.

[22] Siggia, E.D., 1981, Invariants for the one-point vorticity and strain correlation functions. *Physics of Fluids*, **24**, 1934.

[23] Kerr, R.M., 1985, Higher order derivative correlations and the alignment of small-scale structures in isotropic numerical turbulence. *Journal of Fluid Mechanics*, **153**, 31.

[24] Ayyalasomayajula, S. and Warhaft, Z., 2006, Nonlinear interactions in strained axi-symmetric high Reynolds number turbulence *Journal of Fluid Mechanics* (to be published).

[25] Chertkov, M., 2003, Phenomenology of Rayleigh–Taylor turbulence. *Physical Review Letters*, **91**, 115001.